PHYSICAL REVIEW A **80**, 011201(R) (2009)

# Reflective and collateral photoionization of an atom inside a fullerene: Confinement geometry from reciprocal spectra

Matthew A. McCune,[1] Mohamed E. Madjet,[2] and Himadri S. Chakraborty[1,*]
[1]*Department of Chemistry and Physics, Northwest Missouri State University, Maryville, Missouri 64468, USA*
[2]*Institute of Chemistry and Biochemistry, Free University, Fabeckstrasse 36a, D-14195 Berlin, Germany*
(Received 7 May 2009; published 30 July 2009)

In the photoionization of an atom endohedrally confined in a fullerene the electrons directly ionized from the atom partially reflect from the cage. However, the valence atomic electrons can also eject from the cage collaterally with their direct emission. The reflective and the collateral amplitudes oscillate in the electron's momentum space with frequencies determined by their path differences from the direct amplitude. Resulting cross sections reveal the confining geometry in the Fourier conjugate domain. The frequency pattern distinguishes the atomic emission from the fullerene emission.

DOI: 10.1103/PhysRevA.80.011201 PACS number(s): 33.80.Eh, 36.40.Cg, 61.48.−c

A fascinating feature of fullerenes is their hollow interior that can be impregnated with atoms, molecules, and clusters, creating highly sustainable entrapments—the endohedral fullerenes. Vigorous research is being carried out in many different fields to explore applications of these novel materials in nanotechnology. It has been shown that they can make good candidates for the fundamental units of quantum computation [1], the vehicles of pinpoint drug delivery [2], the agents for improved superconduction [3], and the acceptor materials in photovoltaic devices [4]. The knowledge of the spectroscopy of the confined species, therefore, becomes valuable to assess the potential and the limitation of such applications.

Endohedral fullerenes are also natural laboratories for testing traditional science of free atoms in confinement. The photoionization of the confined atom is found to be enhanced by drawing strength from the giant dipole plasmon in the fullerene ionization channels [5–7]. The evidence of hybridization forming atom-fullerene dimer states with unique photo behavior has been found [8]. Detail analysis of these effects was possible using the multielectron description of the fullerene [9]. On the other hand, when modeling the cage by simple static potentials, a rather ubiquitous oscillation in the photoionization of confined atoms has been reported over past several years [10–14]. Calculations in multielectron treatments, such as the molecular dynamical method [15] and the jellium-based density-functional method [16,17], also confirmed this result. On the experimental side, only two total cross-section measurements are performed over the giant $4d$ resonance region of Ce for the neutral [18] and the ionic [19,20] $Ce@C_{82}$. In these, while the presence of oscillations is claimed in the former, no oscillation is detected in the latter. However, given the strong theoretical expectation of the oscillation, more experiments on various other endohedral systems are needed.

As for the origin of the oscillation, the interference of the electron wave emanating directly from the atom with the one reflected from the cage was first suggested in Ref. [14]. While this indeed partly describes the phenomenon, the complete picture should go beyond this. In particular, the atomic outer electron, which transfers some probability density to the cage [5,6], can simultaneously ionize from the cage to enrich the interference effect. In fact, the response of atom-fullerene van-der-Waals-type dimer levels [8] can accentuate such hybrid ionization behavior. The knowledge of the detail mechanism can determine if one could extract geometric information of the confinement from the oscillation, facilitating the analysis of electron spectroscopic measurements of the entrapped atom. Considering $Mg@C_{60}$ as a prototype, we demonstrate that not only the reflected photoelectrons but also "wandering-at-large" *atomic* electrons ejected from the cage, the *collateral* photoelectrons, participate in the interference with powerful effects. Oscillation frequencies, determined by Fourier transforming the cross section, connect to the size of the confinement.

The ground state of $C_{60}$ is constructed using a local-density approximation (LDA) in a spherical frame by delocalizing four valence electrons ($2s^2 2p^2$) from each carbon atom against 60 $C^{4+}$ ions smeared into a jellium [9]. The reliability of the model was demonstrated by providing an excellent description of multiple oscillations in the UV photoionization measurements of $C_{60}$ [21]. We place the Mg atom at the center of $C_{60}$ and obtain the ground state of the combined system [6]. The photoionization cross section $\sigma_{n\ell\to k\ell'}$, for dipole transitions $n\ell \to k(\ell' = \ell \pm 1)$, is given as

$$\sigma_{n\ell\to k\ell'} \sim 2(2\ell+1)|\langle \Phi_{k\ell'}|\delta V|\Phi_{n\ell}\rangle|^2, \qquad (1)$$

where the induced density $\delta V$ includes, besides the dipole interaction, terms representing electron correlations in the time-dependent LDA (TDLDA) [9,22]. Obviously, when the correlation terms are omitted, Eq. (1) yields the independent particle LDA result.

The outermost $3s$ and the inner $2p$ cross sections calculated in TDLDA that includes electron correlations are shown, respectively, in Figs. 1(a) and 1(b) for the confined Mg. Both the curves show oscillations and several narrow spikes from single-electron autoionizations. Ignoring the spikes, the TDLDA curves are very similar to the corresponding LDA curves (shown). This is because over the energy range considered, which is above the $C_{60}$ plasmon re-

*himadri@nwmissouri.edu

 

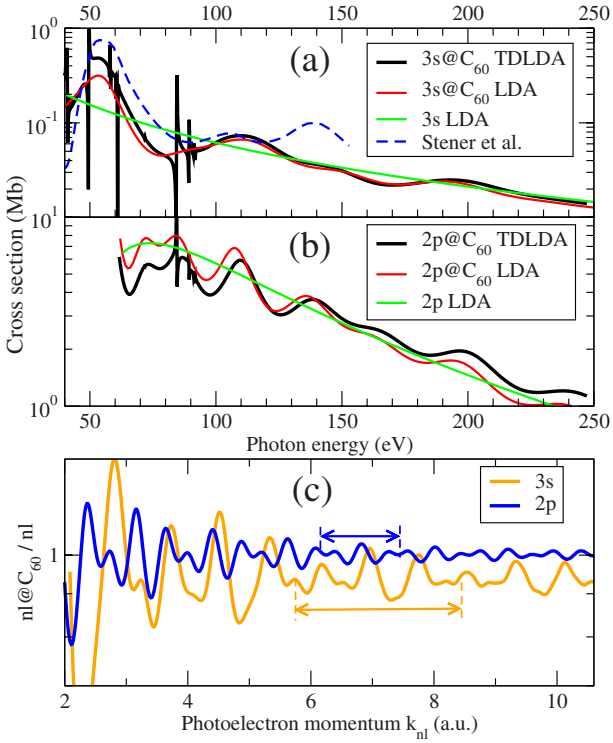


FIG. 1. (Color online) (a) 3*s* TDLDA cross section of confined Mg and LDA results for both confined and free atom. The result from [15] is displayed for comparison. (b) Same as (a) but for Mg 2*p*. (c) Confined-to-free LDA cross-section ratios for 3*s* and 2*p* as a function of the photoelectron momentum. Beating wavelengths are indicated.

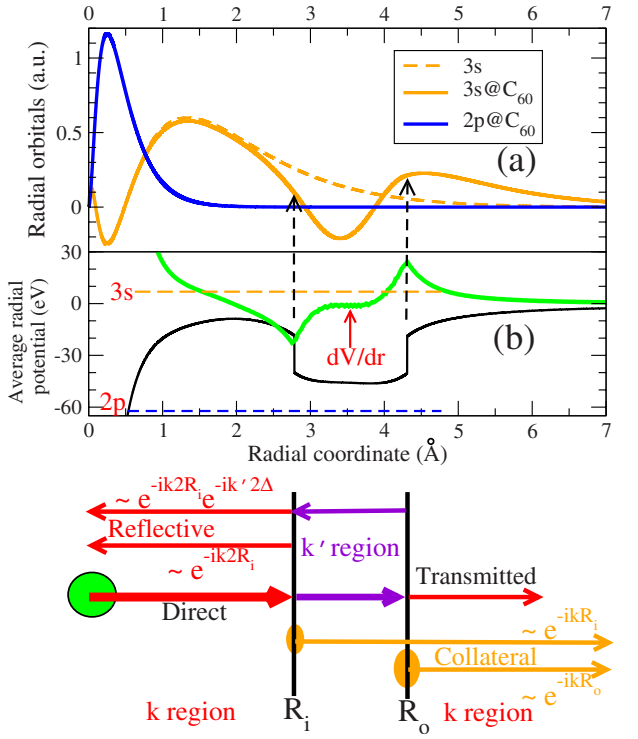


FIG. 2. (Color online) (a) 3*s* wave functions of free and confined Mg and 2*p* wave function of confined Mg. (b) The radial potential of Mg@$C_{60}$ and its derivative. Binding energies of 3*s* and 2*p* of the confined Mg are shown. Bottom: schematic depiction of the photoamplitude at different radial regions.

gion, collective effects practically do not exist. Evidently, the oscillations are single-electron phenomena, and hence we consider the LDA results for our analysis.

Since the LDA cross sections of the confined atom oscillate about their free-atomic counterparts [Figs. 1(a) and 1(b)], a cleaner look at the oscillations is possible by considering the confined-to-free ratio, as the ratio neutralizes the energy-dependent falloff. Ratios for both 3*s* and 2*p* are shown in Fig. 1(c) as a function of corresponding photoelectron momenta, $k_{n\ell}=\sqrt{2(E-E_{n\ell})}$ in atomic units, where $E$ and $E_{n\ell}$ are, respectively, the photon energy and the ionization threshold. Both the curves show smaller oscillations with some superimposed beatings. There, however, exists a major difference. The wavelengths of oscillations are shorter in the 2*p* result; the difference is more dramatic for the beating-type wavelengths as shown in Fig. 1(c). This suggests that the 3*p* and 2*s* cross sections involve distinguishable frequency patterns. In what follows, we unravel the mechanism.

In Fig. 2(b) the LDA radial potential, *averaged* over the occupied orbitals [9], is shown. The potential has edges at the $C_{60}$ inner and outer boundaries: $R_i$=2.79 Å and $R_o$ =4.29 Å, as supported by the experiment [21]. In Fig. 2(a) the LDA radial bound wave functions of 3*s* and 2*p* of confined Mg are shown where 2*p* represents a typical atomic inner-state completely localized at the Mg nucleus. The wave function of the valence 3*s* electron, in contrast, extends further out and is modified by mixing with the $C_{60}$ $\pi$ band [6]. (Technically, with two extra nodes it is 5*s* of the composite system.) Consequently, some 3*s* probability density delocalizes to reside in the cage. This suggests that while the 2*p* electron will solely emerge from the central atom, the 3*s* electron can coemerge from the atomic as well as the cage sites. Before showing the modification in the photoamplitude due to this collateral emergence from the cage, we first analyze the case without it by considering the 2*p* ionization.

Quantum mechanically a part of the electron wave escaping the 2*p* state will reflect from the inner boundary of $C_{60}$, while the other part will enter the cage wall. From the part that enters, a component will further reflect from the outer boundary and the rest will transmit out of the cage. The form of the continuum wave must include these features. We make two simplifications: (i) we are interested in energies above the ionization threshold which implies large photoelectron momenta. Since the Coulomb continuum wave that describes the photoelectron in the regions $0<r<R_i$ and $r>R_o$ approximates the plane wave at large momenta ($k$), we represent the continuum electron by a plane wave. (ii) We disregard the softness of the cage potential at its boundaries and take it as an attractive square well of depth $V_0$.

The radial component of the full continuum wave in Eq. (1) assumes the following forms at different regions:

$$\phi_{\mathrm{DR}}(k,r) = e^{ikr} + \mathcal{R}(k)e^{-ikr}, \quad 0 < r < R_i, \tag{2a}$$

$$\phi_{\mathrm{cage}}(k',r) = C(k')e^{ik'r} + D(k')e^{-ik'r}, \quad R_i < r < R_o, \tag{2b}$$

$$\phi_T(k,r) = \mathcal{T}(k)e^{ikr}, \quad r > R_o, \tag{2c}$$

where the terms on the right of Eq. (2a) denote the direct and the reflected waves respectively with the momentum $k = \sqrt{2(E-E_{2p})}$. $\mathcal{R}$ in Eq. (2a) is the reflective and $\mathcal{T}$ in Eq. (2c) is the transmission coefficient. For the wave inside the cage wall [Eq. (2b)] the kinetic energy measured from the bottom of the well yields the momentum $k' = \sqrt{k^2+2V_0}$. We ignore the continuum angular momentum (determined by the dipole selection), which is a constant phase shift to the plane wave. Matching the waves at $R_i$ and $R_o$ we solve for the coefficients [23]:

$$\mathcal{R}(k) = \frac{i\frac{V_0}{k'k}\sin(k'\Delta)}{\cos(k'\Delta) - i\frac{k'^2+k^2}{2k'k}\sin(k'\Delta)}e^{ik2R_i}, \tag{3a}$$

$$\mathcal{T}(k) = \frac{1}{\cos(k'\Delta) - i\frac{k'^2+k^2}{2k'k}\sin(k'\Delta)}e^{-ik\Delta}, \tag{3b}$$

where the width $\Delta = R_o - R_i$. Exact Eq. (3) satisfy $|\mathcal{R}|^2 + |\mathcal{T}|^2 = 1$ to conserve the photocurrent. For $k > \sqrt{2V_0}$, which will quickly be the case above the threshold, $k' \simeq k + V_0/k$ to the leading order. This approximates the denominator of Eq. (3) to $\exp(-ik'\Delta)$, giving $\mathcal{R}$ in a simplified form:

$$\mathcal{R}(k) \simeq \frac{1}{2}\frac{V_0}{k'k}[-e^{ik2R_i} + e^{ik2R_i}e^{ik'2\Delta}]. \tag{4}$$

The elegance of Eq. (4) is in its explicit display of momentum-dependent phase factors: the former implies the radial path $2R_i$ the electron travels with a momentum $k$ to reflect off the fullerene inner edge, while the later shows an *additional* path of $2\Delta$ with the momentum $k'$ inside the cage wall to bounce off the outer edge.

The $2p$ bound wave function is localized at the central Coulomb region [Fig. 2(a)], indicating that only the continuum wave in the region $0 < r < R_i$ [Eq. (2a)], enters the overlap integral in the ionization amplitude, which, using Eq. (4) and $k' \simeq k + V_0/k$, becomes

$$D_{2p} \sim A^D_{2p}(k) + A^R_{2p}(k)[e^{-ik2R_o}e^{-iV_0(2\Delta/k)} - e^{-ik2R_i}], \tag{5}$$

where $A^D_{2p}$ is the amplitude of the direct ionization which is practically the free atom result. The remaining term in Eq. (5), with $A^R_{2p} = \frac{1}{2}\frac{V_0}{k^2+V_0}A^{D^*}_{2p}$, is the contribution from electrons reflected from the boundaries. This reflective amplitude oscillates in the momentum space with frequencies $2R_i$ and $2R_o$, the effective path differences between the direct and reflected waves, since the effect of $e^{-iV_0 2\Delta/k}$ rapidly weakens with increasing $k$. Note that $A^R$ diminishes with increasing photon energy in inverse quadratic power of $k$.

On the other hand, the overlap integral for the outer $3s$ ionization extends to the cage; see the $3s$ wave function of the confined Mg [Fig. 2(a)]. In this case, while the reflection mechanism continues to exist, a different scenario plays out at the cage, since some $3s$ electrons residing in the cage can collaterally eject. We consider the *acceleration* gauge form $\langle\phi(k,r)|dV/dr|\phi_{3s}\rangle$ of the dipole amplitude used before to study the ionization of free $C_{60}$ [21,24,25]. In this form, the derivative of the potential is a measure of the recoil force available to the escaping electron. We focus only on the overlap at the cage. As shown in Fig. 2(b), $dV/dr$ accumulates at the cage boundaries. This implies dominant photoelectron productions at $r = R_i$ and $r = R_o$, resulting in path differences of $R_i$ and $R_o$, respectively, from the direct atomic emission.

As noted above, for larger $k$ the reflectivity of the cage weakens. This suggests that the outgoing part of Eq. (2b) is dominant above the ionization threshold. Hence, to examine the collateral dynamics it is enough to approximate the ejected wave from the $3s$ level inside the cage wall by $Ce^{ik'r} \simeq Ce^{ikr}e^{iV_0/k}$ at large $k$, where $k = \sqrt{2(E-E_{3s})}$. From the acceleration formalism, we then obtain the amplitude of $3s$ collateral ejection as $A^C_{3s}(k)e^{-iV_0/k}[a_i e^{-ikR_i} - a_o e^{-ikR_o}]$, following Eq. (2) of Ref. [24]. Here $A^C_{3s}$ denotes the energy-dependent decay and $a_i$ and $a_o$ are the values of the $3s$ wave function, respectively, at $R_i$ and $R_o$. The full $3s$ amplitude that also includes the reflective terms as in Eq. (5) then reads

$$D_{3s} \sim A^D_{3s}(k) + A^R_{3s}(k)[e^{-ik2R_o}e^{-iV_0(2\Delta/k)} - e^{-ik2R_i}] + A^C_{3s}(k)e^{-iV_0/k}[a_i e^{-ikR_i} - a_o e^{-ikR_o}]. \tag{6}$$

Obviously, besides $2R_i$ and $2R_o$ from the reflective channel, the $3s$ amplitude contains two additional frequencies, $R_i$ and $R_o$, from the collateral channel. The mechanism is illustrated in the bottom panel of Fig. 2.

The cross section, $\sim|D_{nl}|^2$, is the coherent superposition of the direct, reflective and collateral amplitudes. But since the direct amplitude is large in the absolute value, one can neglect smaller quadratic terms proportional to $|A^R_{nl}|^2$, $|A^C_{nl}|^2$, and $A^{R^*}_{nl}\,A^C_{nl}$ and its complex conjugate (c.c.). Thus, the oscillation in the cross section will dominantly emerge from the interferences of the direct with the reflective and the collateral amplitudes as

$$\sigma_{nl} \approx \sigma^D_{nl} + A^{D^*}_{nl}A^R_{nl}[\cdots] + A^{D^*}_{nl}A^C_{nl}[\cdots] + \text{c.c.} \tag{7}$$

The oscillation is mounted upon a steady background $\sigma^D_{nl} \sim |A^D_{nl}|^2$, which is practically the free atom result. Equation (7) also suggests that the oscillation amplitudes vary linearly with the direct ionization strength (Fig. 1).

Evidently, the cross section contains the same frequencies as in the amplitudes: $2R_i$, $2R_o$ from the reflective and $R_i$, $R_o$ from the collateral emissions. This is in clear contrast to the known oscillations in free $C_{60}$ [21]. In Fig. 3 the Fourier transform magnitudes (FTMs) of $3s$ and $2p$ confined-to-free cross-section ratios are shown. These *reciprocal* spectra yield peaks at the expected radial positions. The height of each peak corresponds to the strength of the respective oscillation via the fore factor in the oscillatory term. From Eqs. (5) and (6), this explains why $2R_i$ and $2R_o$ peaks are of the same strength in both $3s$ and $2p$. In contrast, the oscillation with the frequency $R_o$ from the collateral ejection dominates the $3s$ cross section. This happens because the $3s$ wave function holds a higher value of $a_o$ at $R_o$ [Fig. 2(a)], enabling more $3s$ electrons to liberate from the outer boundary [see Eq. (6)]. In

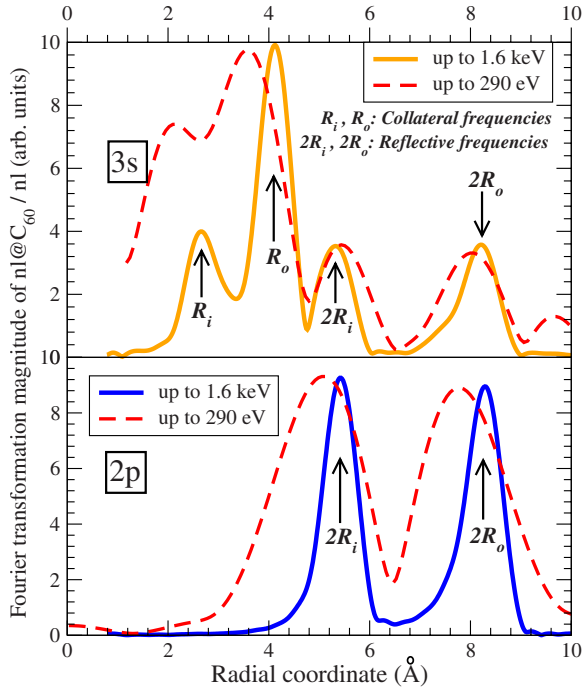


FIG. 3. (Color online) Top: FTM of 3*s* cross-section ratio over extended and limited (up to carbon *K* edge) energy ranges. Bottom: same but for 2*p*.

essence, a strong interplay between reflective and collateral mechanisms entails distinctly varied frequency structures in 3*s* and 2*p* cross sections of the confined Mg.

State-selective measurements of photoelectrons from confined atoms can be carried out by the standard technique of electron spectroscopy. But the photon energy must not intrude on the carbon *K*-shell continuum to ensure little ionization from the $C^{4+}$ core. Hence, we examined if the FTM of cross section ratios for energies *not* exceeding 290 eV is capable of delineating the effect. Barring some offsets, the peak positions are very well reproduced (Fig. 3), implying that the effect should be discernible in the experiment and must be included to interpret the data. Remarkably, since the fullerene cross section has a different system of frequencies [21,26] than the current result, the FTM can be a unique signature of the emission source (i.e., inner, valence, or fullerene level) of the detected photoelectron.

To conclude, we present a complete description of the phenomenon that induces oscillations in the photoionization of an atom in a fullerene. We show that for all the subshells the effect owes to the reflected photoelectrons. For the valence subshell, the effect is further augmented by a stronger participation of the emission collaterally from the cage. As a result, cross sections oscillate in specific frequencies connected to the confinement geometry which can be derived from the reciprocal spectra. Although the effect is illustrated for an encapsulated atom, it must exist for the confined molecules and clusters, multilayer fullerenes, and even for the cylindrical entrapments such as nanopeapods pointing to a far more generic implication of the result.

This work was supported by the NSF. M.E.M. acknowledges supports from CoE UniCat coordinated by TU Berlin and funded by Deutsche Forschungsgemeinschaft.

[1] W. Harneit *et al.*, Phys. Rev. Lett. **98**, 216601 (2007).
[2] J. B. Melanko *et al.*, *Nanotechnology in Drug Delivery*, edited by M. M. de Villiers *et al.* (Springer, New York, 2009), Vol. X, p. 105.
[3] A. Takeda *et al.*, Chem. Commun. (Cambridge) 2006, 912.
[4] R. B. Ross *et al.*, Nature Mater. **8**, 208 (2009).
[5] M. E. Madjet, H. S. Chakraborty, and S. T. Manson, Phys. Rev. Lett. **99**, 243003 (2007).
[6] H. S. Chakraborty, M. E. Madjet, Jan-M. Rost, and S. T. Manson, Phys. Rev. A **78**, 013201 (2008).
[7] M. Ya. Amusia, A. S. Baltenkov, and L. V. Chernysheva, JETP Lett. **87**, 200 (2008).
[8] H. S. Chakraborty, M. E. Madjet, T. Renger, Jan-M. Rost, and S. T. Manson, Phys. Rev. A **79**, 061201(R) (2009).
[9] M. E. Madjet, H. S. Chakraborty, Jan-M. Rost, and S. T. Manson, J. Phys. B **41**, 105101 (2008).
[10] M. Ya. Amusia, A. S. Baltenkov, and L. V. Chernysheva, Phys. Rev. A **75**, 043201 (2007), and references therein.
[11] H. R. Varma, P. C. Deshmukh, V. K. Dolmatov, and S. T. Manson, Phys. Rev. A **76**, 012711 (2007).
[12] A. Lyras and H. Bachau, J. Phys. B **38**, 1119 (2005).
[13] A. S. Baltenkov, V. K. Dolmatov, and S. T. Manson, Phys. Rev. A **66**, 023201 (2002).
[14] J.-P. Connerade, V. K. Dolmatov, and S. T. Manson, J. Phys. B **33**, 2279 (2000).
[15] M. Stener *et al.*, J. Phys. B **35**, 1421 (2002).
[16] G. Wendin and B. Wästberg, Phys. Rev. B **48**, 14764 (1993).
[17] M. J. Puska and R. M. Nieminen, Phys. Rev. A **47**, 1181 (1993).
[18] K. Mitsuke *et al.*, J. Chem. Phys. **122**, 064304 (2005).
[19] A. Müller *et al.*, J. Phys.: Conf. Ser. **88**, 012038 (2007).
[20] A. Müller *et al.*, Phys. Rev. Lett. **101**, 133001 (2008).
[21] A. Rüdel, R. Hentges, U. Becker, H. S. Chakraborty, M. E. Madjet, and J. M. Rost, Phys. Rev. Lett. **89**, 125503 (2002).
[22] S. Saito, G. F. Bertsch, and D. Tománek, Phys. Rev. B **43**, 6804 (1991).
[23] F. S. Levin, *An Introduction to Quantum Theory* (Cambridge University Press, Cambridge, 2002), p. 255.
[24] M. A. McCune, M. E. Madjet, and H. S. Chakraborty, J. Phys. B **41**, 201003 (2008).
[25] O. Frank and J. M. Rost, Chem. Phys. Lett. **271**, 367 (1997).
[26] T. Liebsch *et al.*, Chem. Phys. Lett. **279**, 197 (1997).